Science
AAAS

Mode Locking of Electron Spin Coherences in Singly Charged Quantum Dots

A. Greilich, *et al.*

Science **313**, 341 (2006);
DOI: 10.1126/science.1128215

This copy is for your personal, non-commercial use only.

If you wish to distribute this article to others, you can order high-quality copies for your colleagues, clients, or customers by clicking here.

Permission to republish or repurpose articles or portions of articles can be obtained by following the guidelines here.

The following resources related to this article are available online at www.sciencemag.org (this information is current as of May 28, 2010):

Updated information and services, including high-resolution figures, can be found in the online version of this article at:
http://www.sciencemag.org/cgi/content/full/313/5785/341

Supporting Online Material can be found at:
http://www.sciencemag.org/cgi/content/full/313/5785/341/DC1

This article **cites 15 articles**, 2 of which can be accessed for free:
http://www.sciencemag.org/cgi/content/full/313/5785/341#otherarticles

This article has been **cited by** 107 article(s) on the ISI Web of Science.

This article has been **cited by** 2 articles hosted by HighWire Press; see:
http://www.sciencemag.org/cgi/content/full/313/5785/341#otherarticles

This article appears in the following **subject collections**:
Physics, Applied
http://www.sciencemag.org/cgi/collection/app_physics

Downloaded from www.sciencemag.org on May 28, 2010

Science (print ISSN 0036-8075; online ISSN 1095-9203) is published weekly, except the last week in December, by the American Association for the Advancement of Science, 1200 New York Avenue NW, Washington, DC 20005. Copyright 2006 by the American Association for the Advancement of Science; all rights reserved. The title *Science* is a registered trademark of AAAS.

Laboratories Laboratory Directed Research and Development program, the Army Research Office (DAAD 19-03-1-227), and the NIH Nanomedicine Center Program (#206-00139-06). We acknowledge P. Calvert for discussions of ink-jet printing. Images in this paper were generated in the University of New Mexico Cancer Center Fluorescence Microscopy Facility, supported as detailed at http://kugrserver.health.unm.edu:16080/microscopy/facility.html. Use of the Advanced Photon Source was supported by the U.S. Department of Energy, Office of Science, Office of Basic Energy Sciences, under Contract No. W-31-109-ENG-38. Sandia is a multiprogram laboratory operated by Sandia Corporation, a Lockheed Martin Company, for the U.S. Department of Energy's National Nuclear Security Administration under Contract DE-AC04-94AL85000.

Supporting Online Material
www.sciencemag.org/cgi/content/full/313/5785/337/DC1
Materials and Methods
Figs. S1 to S5
References

23 February 2006; accepted 1 June 2006
10.1126/science.1126590

Mode Locking of Electron Spin Coherences in Singly Charged Quantum Dots

A. Greilich,[1] D. R. Yakovlev,[1,2]* A. Shabaev,[3,4] Al. L. Efros,[3]* I. A. Yugova,[1,5] R. Oulton,[1] V. Stavarache,[6] D. Reuter,[6] A. Wieck,[6] M. Bayer[1]*

The fast dephasing of electron spins in an ensemble of quantum dots is detrimental for applications in quantum information processing. We show here that dephasing can be overcome by using a periodic train of light pulses to synchronize the phases of the precessing spins, and we demonstrate this effect in an ensemble of singly charged (In,Ga)As/GaAs quantum dots. This mode locking leads to constructive interference of contributions to Faraday rotation and presents potential applications based on robust quantum coherence within an ensemble of dots.

Electron spins in ensembles of quantum dots (QDs) offer one possible pathway to implementing quantum information technologies in a solid-state environment (*1*–*4*). Unfortunately, inhomogeneities within an ensemble lead to the rapid loss of coherence among the phases of the spins, typically on the scale of nanoseconds (*5*–*7*). This is orders of magnitude shorter than the coherence time for a single QD, which can be as long as microseconds (*8*). Theoretically, the single-spin coherence time can be even longer, in principle up to twice the spin relaxation time (*9*), which is on the scale of milliseconds (*10*, *11*). The fast dephasing in an ensemble is due to both spatial fluctuations in the nuclear magnetic fields (*12*, *13*) and inhomogeneities in the electron *g* factor (*3*). These effects may be overcome by sophisticated spin-echo techniques (*14*), but a simple and robust technique for preserving spin coherence could ultimately enable many of the operations that are critical to the processing of quantum information, including initialization, manipulation, and read-out of a coherent spin state.

Here we report an optical technique based on time-resolved Faraday rotation (FR) measurements of the electron spin dynamics in an ensemble of QDs to recover the coherence time of a single QD. A periodic train of circularly polarized light pulses from a mode-locked laser synchronizes the precession of the spins to the laser repetition rate, transferring the mode-locking into the spin system. This synchronization leads to constructive interference of the electron spin polarization in time. The interference also gives the possibility for all-optical coherent manipulation of spin ensembles: The electron spins can be clocked by two trains of pump pulses with a fixed temporal delay. After this pulse sequence, the QD ensemble shows multiple echo-like FR signals with a period equal to the pump pulse separation.

The experiments were performed on self-assembled (In,Ga)As/GaAs QDs prepared such that each dot contains on average a single electron (*16*) [Supporting Online Material (SOM) Text]. The full width at half maximum of the photoluminescence emission line is 15 meV (Fig. 1B). We used a mode-locked laser that emits pulses with 1.5-ps duration at a rate of 75.6 MHz, corresponding to a pulse separation of T_R = 13.2 ns. In the pump-probe FR with picosecond resolution, spin coherence is generated by a circularly polarized pump pulse, and this coherence is monitored through the precession of the spins about a magnetic field that is applied perpendicular to the structure growth axis (Fig. 1A). For this monitoring, a subsequent linearly polarized probe pulse is used; the beam polarization is rotated due to circular birefringence of the dots that is induced by the photogenerated spin polarization (SOM Text).

In Fig. 1C, FR signals of the QDs are shown as a function of delay between pump and probe at different magnetic fields B. At B = 0, a single, strongly damped oscillation is seen at positive delays after the pump pulse arrival at time t = 0. This signal arises from light scattering by the spin-polarized photoinduced carriers, which together with the residual electron form a negatively charged exciton (trion). No signal is detected at negative delays ($t < 0$). In a magnetic field of 1 T, long-lived electron spin quantum beats appear at positive delays. From the weak decay of the FR signal with increasing delay, a spin dephasing time T_2^* of up to 2 ns can be estimated at low fields. Because this time is much longer than the 400-ps lifetime of the electron-hole pairs injected by the pump pulse (*15*), the beats are due to the spin precession of the residual electrons in the QDs with a frequency $\omega_e = g_e \mu_B B/\hbar$, where μ_B is the Bohr magneton and $\hbar$ is Planck's constant divided by 2π. $|g_e| = 0.57$ is the electron *g* factor (*16*). For a magnetic field of 6 T, an additional modulation of the FR signal appears at short positive delays, whose decay during 400 ps matches the electron-hole lifetime. This modulation arises from interference of spin precessions of the residual electron and the photoexcited carriers (*16*).

The long-lived beats in the FR signal at positive delays are due to initialization of spin coherency of the residual QD electrons by the pump pulses that are resonant with the trion. If the electron spin precession is slow in the limit of weak or zero magnetic field such that $\omega_e \tau_r \ll 1$, where τ_r is the trion lifetime, then the coherency is nullified after trion recombination (*16*–*18*). In the opposite case of fast spin precession ($\omega_e \tau_r \gg 1$), the spin coherence is controlled by the pump pulse area (*16*). For that situation, Rabi-oscillations of the FR amplitude have been reported for the studied structures (*16*) for which the residual electron spin coherence reaches maximum for pulses with area π.

Under these conditions, strong spin quantum beats with a frequency corresponding to the electron precession are observed also at negative delays in a nonzero magnetic field. The amplitude of these quantum beats increases when approaching zero delay t = 0. Spin beats at negative delay have been reported for experimental situations in which the decay time exceeds the time interval between the pump pulses: $T_2^* \geq T_R$ (*3*). This is clearly not the case here, where the FR signal has fully vanished after 1.2 ns at B = 6 T, so that $T_2^* < T_R$.

The FR traces were analyzed for positive and negative delays by exponentially damped oscillatory functions. The magnetic field dependencies of the decay time T_2^* of the ensemble spin precession are given in Fig. 1D. The varia-

[1]Experimentelle Physik II, Universität Dortmund, D-44221 Dortmund, Germany. [2]A. F. Ioffe Physico-Technical Institute, 194021 St. Petersburg, Russia. [3]Naval Research Laboratory, Washington, DC 20375, USA. [4]School of Computational Sciences, George Mason University, Fairfax, VA 22030, USA. [5]Institute of Physics, St. Petersburg State University, 198504, St. Petersburg, Russia. [6]Angewandte Festkörperphysik, Ruhr-Universität Bochum, D-44780 Bochum, Germany.

*To whom correspondence should be addressed. E-mail: dmitri.yakovlev@physik.uni-dortmund.de (D.R.Y.); efros@dave.nrl.navy.mil (Al.L.E.); manfred.bayer@physik.uni-dortmund.de (M.B.)

Downloaded from www.sciencemag.org on May 28, 2010

tions Δg_e of the electronic g factor in the ensemble are translated into variations of the precession frequency, $\gamma \equiv \Delta\omega_e = \sqrt{2}\Delta g_e \mu_B B/\hbar$, which becomes larger with increasing magnetic field. This is the dominant contribution to the enhanced dephasing with increasing field. From a fit to the T_2^* data that is proportional to B^{-1} (the solid line in Fig. 1D), we estimate the g factor dispersion to be $\Delta g_e \approx 0.005$, within the energy window of QDs excited by the laser. The coincidence of the dephasing times T_2^* for $t > 0$ and $t < 0$ gives us a clear hint that it is the same spin system—the residual electrons in the n-type doped QDs—which is responsible for the FR at positive and negative delays.

The negative delay precession can occur only if the coherence of the electron spin in each single dot prevails for much longer times than the time interval T_R between the laser pump pulses, in contrast with the ensemble spin dephasing. Therefore, the dependence of the FR amplitude at negative delay on the pump pulse repetition period may provide information on the spin coherence time of a single QD, T_2. The corresponding data at $B = 6$ T measured for two pump densities differing by a factor of two are given in Fig. 1E. The repetition period T_R was increased from 13.2 ns up to 990 ns by means of a laser pulse picker. A significant FR signal can be measured even for the longest pulse interval of a microsecond, which is comparable to the recently measured electron coherence time T_2 in a gated single QD (*8*).

To understand why the single QD coherence time can be seen in an ensemble measurement, let us consider excitation of a single QD by a periodic π pulse train of circularly polarized light. The first impact of the pulse train is a synchronization of electron spin precession. For discussing this effect, we define the degree of spin synchronization by $P(\omega_e) = 2|S_z(\omega_e)|$. Here $S_z(\omega_e)$ is the z projection of the electron spin at the moment of pulse arrival. It was shown theoretically that if the pulse period T_R is equal to an integer number N times the electron spin precession period in transverse magnetic field $2\pi/\omega_e$, such a train of π pulses leads to almost 100% electron spin alignment along the direction of light propagation (*17*). As a result, the degree of spin synchronization reaches its largest value $P_\pi = \exp(-T_R/T_2)/[2 - \exp(-T_R/T_2)]$, corresponding to almost 100% synchronization. This is because for excitation with a high repetition rate (as in experiment), $T_R \ll T_2$ so that $\exp(-T_R/T_2) \approx 1$.

An ensemble contains QDs whose precession frequencies fulfill the phase synchronization condition (PSC)

$$\omega_e = 2\pi N/T_R \equiv N\Omega \qquad (1)$$

Generally, multiple QD subsets satisfy the condition Eq. 1 for different N within the whole ensemble. This is due to the wide distribution of spin precession frequencies for the optically oriented electrons, γ, caused by the dispersion of g factors in Fig. 1B. This is illustrated by Fig. 2, where panel A sketches the precession for $N = K$ and $K + 1$, where K is a large integer, and panel B gives the spectrum of phase synchronized precession modes. The number of synchronized subsets ΔN can be estimated from the broadening of the electron spin precession frequencies by $\Delta N \sim \gamma/\Omega$. It increases linearly with magnetic field B and pulse period T_R. The spins in each subset precess between the pump pulses with frequency $N\Omega$, starting with an initial phase that is the same for all subsets. The spins' contribution to the spin polarization of the ensemble at a time t after the pulse is given by $-0.5\cos(N\Omega t)$. As sketched in Fig. 2A, the sum of oscillating terms from all subsets leads to constructive interference of their contributions when the next pulse arrives. The rest of the QDs do not contribute to the average electron spin polarization $\overline{S}_z(t)$ at times $t \gg T_2^*$ due to dephasing. The average spin polarization can be written as $\overline{S}_z(t) = -0.5\Omega \sum_{N=-\infty}^{\infty} \cos(N\Omega t)\rho(N\Omega)$, where $\rho(\omega_e)$ is the density of the QD precession frequencies within the laser excitation profile. Assuming that this density has a Lorentzian shape (*19*) $\rho(\omega_e) = (\gamma/\pi)[1/(\{\omega_e - \overline{\omega}_e\}^2 + \gamma^2)]$, cen-

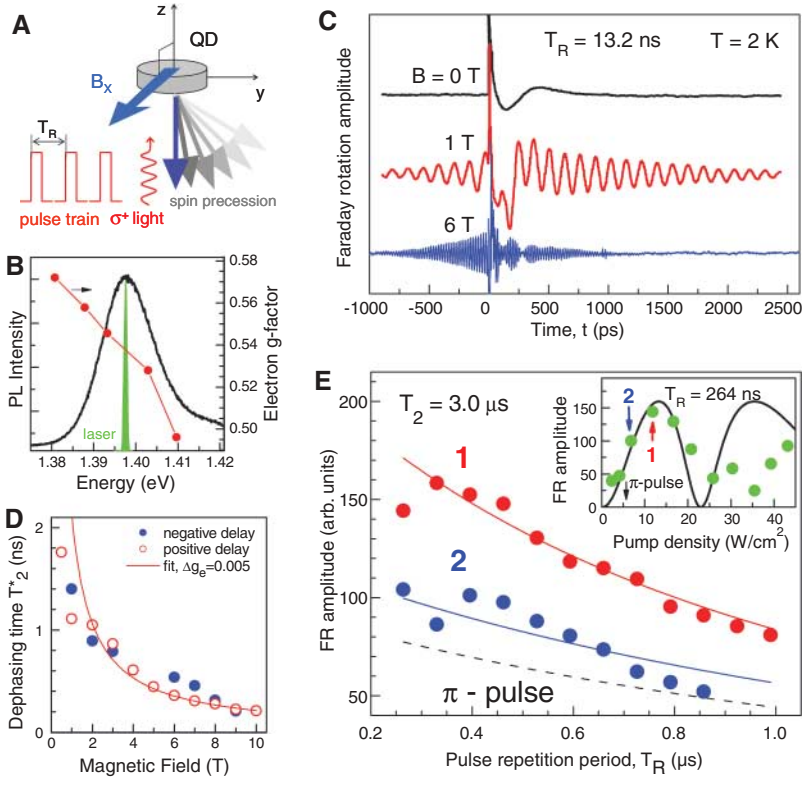

Fig. 1. (**A**) Geometry of experiment. The electron spin precession in a transverse magnetic field is excited by the train of short pulses of circularly polarized light. (**B**) Photoluminescence (PL) spectrum of the studied (In,Ga)As/GaAs dot ensemble measured at temperature $T = 2$ K. The spectrum of the pulsed laser with a spectral width of about 1 meV used for pumping and probing is shown by the green area. The symbols give the variation of the electron g factor across the inhomogeneously broadened emission spectrum (line is guide to the eye). (**C**) Pump-probe FR signal measured at different magnetic fields on singly charged (In,Ga)As/GaAs QDs. The pump power density is 60 W/cm² and the probe density is 20 W/cm². For nonzero fields, distinct oscillations are seen at positive and negative delays due to Larmor precession of electron spins about the magnetic field. (**D**) Dephasing time T_2^* evaluated for positive (open circles) and negative (solid circles) delays as function of magnetic field. The solid line is a fit to the experimental data with a function $T_2^* \propto [\hbar\sqrt{2}]/(\Delta g_e\ \mu_B\ B)$ in order to evaluate $\Delta g_e \approx 0.005$. (**E**) FR amplitude at negative delay as function of time interval between pump pulses. The experimental data were measured at $B = 6$ T for two pump densities of 12 and 6 W/cm² shown in the inset by the red and blue arrows, respectively. The temperature $T = 6$ K. The solid lines show the theoretical dependencies described by Eq. B11, which contained as single fit parameter $T_2 = 3.0$ μs. In the inset, the FR amplitude measured at $T_R = 264$ ns is shown as function of pump density. The solid line shows the theoretical dependence described by Eq. B11. The comparison of experiment and theory allows us to determine the pump density, which corresponds to the π pulse (shown by the black arrow). The theoretical dependence of the FR amplitude on T_R calculated for π pulse excitation is shown by the dashed line.

Downloaded from www.sciencemag.org on May 28, 2010

tered around the average frequency $\overline{\omega}_e$, we obtain

$$\overline{S}_z(t) \approx \frac{\beta\cosh\{\beta[1 - 2\mathrm{mod}(t, T_R)]\} - \sinh\beta}{\beta\sinh\beta} \times \cos(\overline{\omega}_e t) \quad (2)$$

where $\beta = \gamma T_R/2$ and $\mathrm{mod}(x, y) = x - y[x/y]$ is the modul function, with $[x/y]$ defined as integer division. The resulting time dependence of $\overline{S}_z(t)$ (Fig. 2A) explains the appearance of FR signal at negative delays.

π pulse excitation is not critical for the electron spin phase synchronization by the train of circularly polarized light pulses. Resonant pulses of arbitrary intensity create a coherent superposition of the trion and electron state in a QD (*16*), leading to a long-lived coherence of resident electron spins, because the coherence is not affected by the radiative decay of the trion component. Each pulse of σ^+ polarized light changes the electron spin projection along the light propagation direction by $\Delta S_z = -[1 - 2|S_z(t \to t_n)|]W/2$, where $t_n = nT_R$ is the time of the nth pulse arrival and $W = \sin^2(\Theta/2)$, with Θ being the pulse area (*16*, *18*). Consequently, a train of these pulses orients the electron spin opposite to the light propagation direction, and it also increases the degree of electron spin synchronization P. The application of pulses with $\Theta = \pi$ (corresponding to $W = 1$) leads to a 99% degree of electron spin synchronization after only a dozen pulses (*17*). However, if the electron spin coherence time is long enough ($T_2 \gg T_R$), an extended train of pulses leads to a high degree of spin synchronization even for $\Theta \ll 1$ ($W \approx \Theta^2/4$). The general consideration of this problem in the SOM Text (Eq. B6) gives a degree of synchronization $P(\omega_e) = 2|S_z(\omega_e)|$

$$P(\omega_e) = \frac{(W/2T_R)(W/2T_R + 1/T_2)}{(W/2T_R + 1/T_2)^2 + (\omega_e - N\Omega)^2} \quad (3)$$

One sees the following: (i) A train of pulses synchronizes the spin precession of QD electrons with precession frequencies in a narrow range of width $W/2T_R + 1/T_2$ around the PSC. (ii) The electron spin synchronization still reaches 100% if $W/2T_R \gg 1/T_2$.

In case of $\Theta = \pi$, Eq. B7 gives the degree of the electron spin synchronization as

$$P_\pi(\omega_e) = \frac{e^{-T_R/T_2}|\cos(2\pi\omega_e/\Omega)|}{2 - e^{-T_R/T_2}\cos(2\pi\omega_e/\Omega)} \quad (4)$$

corresponding to the maximum degree of spin synchronization P_π for electrons matching the PSC. π pulses synchronize the electron spin precession in a broad range of frequencies with width ~ Ω, which is about equal to the gap between neighboring PSC frequencies.

The effect of the pump density (namely of the pump area) on the distribution of the spin polarization synchronized by and with the pulse train at moment of the pulse arrival ($t = t_n$) for $\Theta = 0.4\pi$, π, and 1.6π is shown in Fig. 3, A to C. Calculations were done for $T_R = 13.2$ ns (red) and 52.8 ns (blue). The density of the electron spin precession modes is shown by the black line, which gives the envelope of the spin polarization distribution. The quasi-discrete structure of the distribution created by the pulse train is the most important feature, which allows us to measure the long spin coherence time of a single QD on an ensemble. A continuous density of spin precession modes would always cause fast dephasing with a time inversely proportional to the total width of the frequency distribution: $T_2^* = \hbar/\gamma$. Only the gaps in the density of precession modes facilitate the constructive interference at negative delay times in Fig. 1C. These gaps are created by mode locking of the electron spins with the periodic laser emission.

The broadening of the quasi-discrete spectra around the PSC is significantly smaller than γ; nevertheless, it leads to dephasing. The calculations in the SOM show that the dephasing rate of the QD ensemble can be written as $\Gamma + 1/T_2$, where the additional dephasing rate Γ depends on T_2, W, and T_R as seen from Eq. B12. In the present limit of $T_R \ll T_2$, Eq. B12 gives $\Gamma \approx W/2T_R + 1/T_2$ and $\Gamma \approx \ln(2 + \sqrt{3})/T_R + 1/T_2$ for $W \ll 1$ and $W = 1$, respectively. Γ is obviously smaller for weak excitation pulses. These results are consistent with the fact that the dephasing is inversely proportional to the broadening of the phase-matched precession modes.

Figure 3D shows the decay of the normalized FR amplitudes as a function of pulse repetition time T_R and calculated using Eq. B11. The decay depends on the pulse area and is minimized for a π pulse. The decay rate for pulses with areas deviating from π are equal for $\Theta = \pi - \alpha$ and $\pi + \alpha$, where α is the deviation from a π pulse ($0 < \alpha < \pi$). We have fitted the experimental dependence of the FR amplitude on T_R (Fig. 1E) and its dependence on pump density (Fig. 1E, inset) by Eq. B11. The factor two difference in pumping intensities used for recording the data labeled 1 and 2 leads to a significant restriction of the T_2 value in Fig. 1E. The fit allows us to determine a pump density corresponding to the π pulse and a single quantum dot coherence time $T_2 = 3.0 \pm 0.3$ μs, which is four orders of magnitude longer than the ensemble dephasing time $T_2^* = 0.4$ ns at $B = 6$ T.

The FR amplitude does not reach its largest value at π pulse pumping (Fig. 1E, inset). This is because the train of π pulses synchronizes the spin precession for a broad distribution of precession frequencies and not only for the ω_e satisfying the PSC. For example, in the QDs with $\omega_e = (N + 1/2)\Omega$, the spin synchronization degree is 1/3 (Eq. 4). However, the S_z projection of electron spin in these QDs is opposite to the one for QDs which satisfy the PSC ($\omega_e = N\Omega$) (Fig. 3B). This leads to cancellation effects in the total FR amplitude

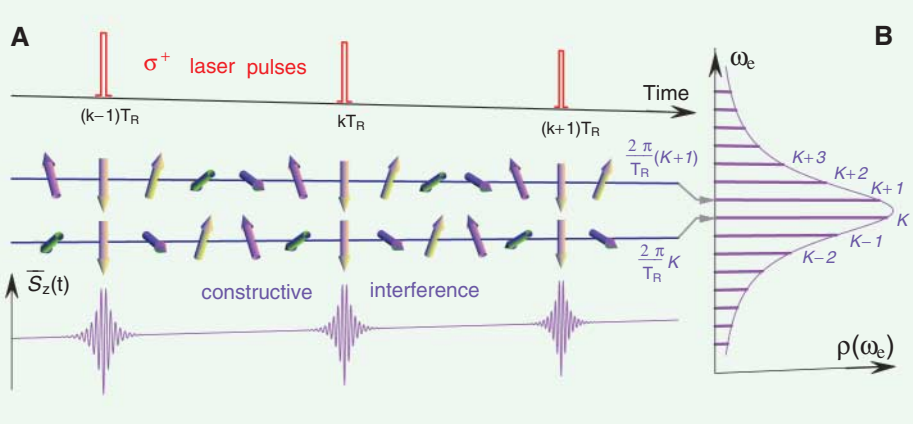

Fig. 2. (**A**) Phase synchronization of electron spin precession by a train of π pulses of circularly polarized light. The top panel shows the train of σ^+ polarized laser pulses with repetition period T_R. The train synchronizes the electron spin precession in QDs, where the precession frequency is a multiple of $(2\pi/T_R)$: $\omega_e = N(2\pi/T_R)$. In these QDs, the spins are aligned at the moment of the pulse arrival; each spin is opposite to the light propagation direction. The two middle panels show the phase synchronization for two spins with precession frequencies differing by $2\pi/T_R$: $N = K$ and $N = K + 1$ (K is a large integer). The bottom panel shows a time evolution of the average spin polarization $\overline{S}_z(t)$, resulting from a constructive interference of the phase synchronized QD subsets. (**B**) Spectrum of phase-synchronized electron spin precession modes enveloped by the density of precession frequencies $\rho(\omega_e)$ in a QD ensemble. Only those electron spins that are synchronized by the pulse train give a contribution to the spectrum, consisting of sharp peaks at the frequencies $\omega_e = N(2\pi/T_R)$ ($N = \ldots, K - 1, K, K + 1, \ldots$), which satisfy the phase synchronization condition Eq. 1.

Downloaded from www.sciencemag.org on May 28, 2010

of the QD ensemble. In contrast, one can see in Fig. 3C that pulses with an area $\Theta > \pi$ are not so efficient in synchronizing the electron spin precession in QDs that do not satisfy the PSC. This diminishes the "negative" contribution of such QDs to the electron spin polarization and increases the FR amplitude. Generally, the rise of the excitation intensity from zero to π pulses increases the number of QDs contributing to the FR signal at negative delays.

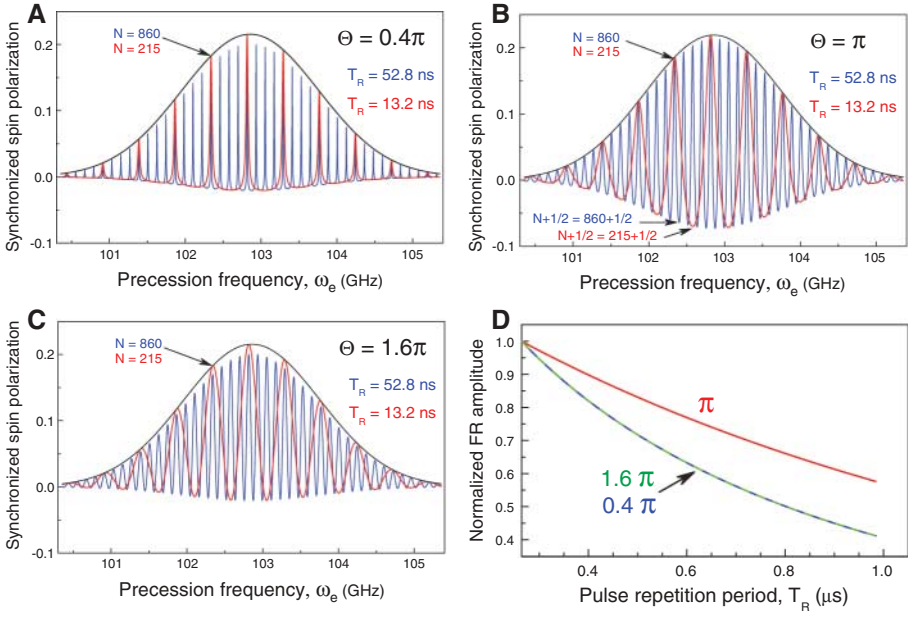

Fig. 3. (**A** to **C**) Spectra of phase-synchronized electron spin precession modes created by a train of circularly polarized pulses, $-\bar{S}_z(t_n)$, calculated for the pulse area $\Theta = 0.4\pi$, π, and 1.6π, respectively. The spectra have been calculated for two pump pulse repetition periods: $T_R = 13.2$ ns (red) and 52.8 ns (blue). At low pumping intensity (A), the pulse train synchronizes electron spin precession in a very narrow frequency range near the PSC: $\omega_e = N(2\pi/T_R)$. The π pulses (B) widen the range of synchronized precession frequencies. In addition, the electron spins with opposite polarization at frequencies between the PSC become significantly synchronized. The degree of synchronization for these spins decreases at $\Theta > \pi$ (C). (**D**) Negative delay FR amplitude dependence on pump pulse repetition period T_R calculated for the same three pulse areas. The amplitude is normalized to its value at $T_R = 264$ ns. The normalized FR amplitude shows the slowest decay for the π pulse excitation. The decay rates are equal for pulses with areas $\Theta = \pi - \alpha$ and $\Theta = \pi + \alpha$, where $\alpha < \pi$. All calculations have been done for a magnetic field of $B = 2$ T with $g_e = |0.57|$, $\Delta g_e = 0.005$, and $T_2 = 3.0$ μs.

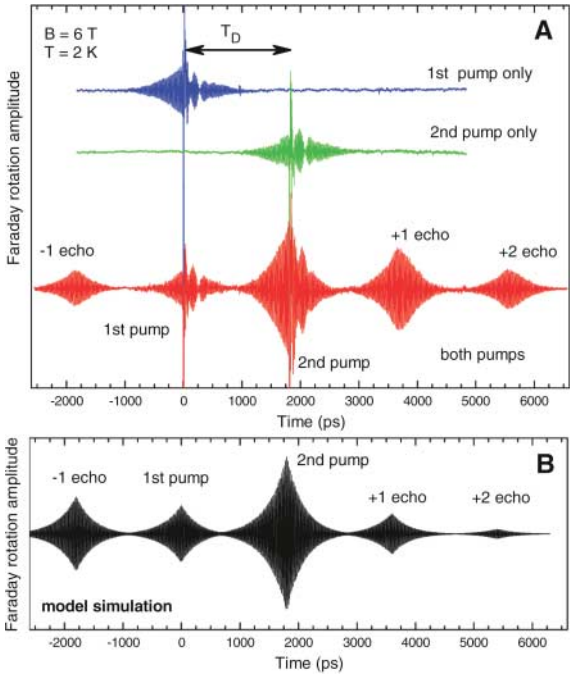

Fig. 4. Control of electron spin synchronization by two trains of pump pulses with $T_R = 13.2$ ns shifted in time by $T_D = 1.84$ ns. (**A**) Experimental FR measured for separate action of the 1st or the 2nd pump (the two upper curves) and for joint action of both pumps (the bottom curve). Pumps were copolarized (σ^+). The joint action of the two pumps leads to the echo-like responses before the first and after the second pump pulse. (**B**) Theoretical modeling of the spin echo–like signals in the two-pulse experiment. Parameters: $\Theta = \pi$ and $\gamma = 3.2$ GHz.

After showing that a specific protocol for a laser pulse sequence can be used for selecting a subset of synchronized QDs with the single dot dephasing time, we turn to testing the degree of control that can be achieved by such sequences. For that purpose, each pump is split into two pulses with a fixed delay $T_D < T_R$ between them. The results of measurements for $T_D = 1.84$ ns are plotted in Fig. 4A. Both pumps were circularly copolarized and had the same intensities. When the QDs are exposed to only one of the two pumps (the two upper traces), the FR signals are identical except for a shift by T_D. The signal changes drastically under excitation by the two-pulse train (the lower trace). Around the arrival time of pump 1, the same FR response is observed as before in the one-pump experiment. Also around pump 2, qualitatively the same FR pattern is observed with considerably larger amplitude. Therefore the coherent response of the synchronized QD ensemble can be amplified by the second laser pulse. Even more remarkable are the echo-like responses showing up in the FR signal before the first and after the second pump pulse. They have a symmetric shape with the same decay and rise times T_2^*. The temporal separation between them is a multiple of T_D. These echo signals show no additional modulation of the FR traces as seen at positive delay times when the pump is applied. This is in agreement with the assignment of the modulation to the photogenerated carriers (*16*).

Apparently, the electron spins in the QD subensemble, which is synchronized with the laser repetition rate, have been clocked by introducing a second frequency, which is determined by the laser pulse separation. The clocking results in multiple echoes in the FR response. This behavior can be explained by our theoretical model: The echo-like signal has the same origin as the FR revival in the single-pump experiment, which is constructive interference of the FR amplitudes from QD subsets with phase-synchronized electron spin precession. We have calculated the distribution of electron spin polarization created by a train of π pulses in the two-pump experiment by using a technique similar to the one described in the SOM for the single pump experiment. The resultant time dependence of the FR signal reproduces the experimental echo signals well (Fig. 4B).

Phase synchronization of the electron spin precession modes in a QD ensemble by a laser pulse train reveals the long spin coherence time of a single dot. Two-pump experiments demon-

Downloaded from www.sciencemag.org on May 28, 2010

strate the opportunity to control the spin ensemble's coherent response by tailoring the desirable time response. The phase synchronization is "robust," because it allows one to exploit all advantages of working with a QD ensemble for "hardware" components in spintronics or quantum information: (i) a strong detection signal with relatively small noise can be recorded and (ii) changes of external parameters such as repetition rate and magnetic field strength can be accommodated in the PSC due to the broad distribution of electron spin precession frequencies in the ensemble and the large number of involved QDs.

References and Notes

1. D. Loss, D. P. DiVincenzo, *Phys. Rev. A.* **57**, 120 (1998).
2. A. Imamoglu *et al.*, *Phys. Rev. Lett.* **83**, 4204 (1999).
3. D. D. Awschalom, D. Loss, N. Samarth, Eds., *Semiconductor Spintronics and Quantum Computation* (Springer-Verlag, Heidelberg, 2002).
4. S. A. Wolf *et al.*, *Science* **294**, 1488 (2001).
5. M. V. Gurudev Dutt *et al.*, *Phys. Rev. Lett.* **94**, 227403 (2005).
6. A. S. Bracker *et al.*, *Phys. Rev. Lett.* **94**, 047402 (2005).
7. P.-F.-Braun *et al.*, *Phys. Rev. Lett.* **94**, 116601 (2005).
8. J. R. Petta *et al.*, *Science* **309**, 2180 (2005).
9. W. A. Coish, D. Loss, *Phys. Rev. B* **70**, 195340 (2004).
10. J. M. Elzerman *et al.*, *Nature* **430**, 431 (2004).
11. M. Kroutvar *et al.*, *Nature* **432**, 81 (2004).
12. I. A. Merkulov, Al. L. Efros, M. Rosen, *Phys. Rev. B* **65**, 205309 (2002).
13. A. V. Khaetskii, D. Loss, L. Glazman, *Phys. Rev. Lett.* **88**, 186802 (2002).
14. C. P. Slichter, *Principles of Magnetic Resonance* (Springer-Verlag, Berlin, 1996).
15. A. Greilich *et al.*, *Phys. Rev. B* **73**, 045323 (2006).
16. A. Greilich *et al.*, *Phys. Rev. Lett.* **96**, 227401 (2006).
17. A. Shabaev, Al. L. Efros, D. Gammon, I. A. Merkulov, *Phys. Rev. B* **68**, 201305(R) (2003).
18. T. A. Kennedy *et al.*, *Phys. Rev. B* **73**, 045307 (2006).

19. We chose a Lorentzian profile for the QD precession frequencies in the consideration because it leads to the closed form for $\bar{S}_z(t)$ in Eq. 2. Generally, our numerical calculations do not show any qualitative or quantitative differences for either the Gaussian or the Lorentzian profiles as long as the distribution $\rho(\omega_e)$ is smoothly going to zero on the scale of its width.

20. We are grateful to S. Erwin for his critical suggestions on the manuscript. This work was supported by the Bundesministerium für Bildung und Forschung program nanoquit, the Defense Advanced Research Projects Agency program QuIST, the Office of Naval Research, and the Deutsche Forschungsgemeinschaft (Forschergruppe Quantum Optics in Semiconductor Nanostructures). R. O. thanks the Alexander von Humboldt foundation.

Supporting Online Materials

www.sciencemag.org/cgi/content/full/313/5785/341/DC1
SOM Text
References

3 April 2006; accepted 14 June 2006
10.1126/science.1128215

Large Wind Shift on the Great Plains During the Medieval Warm Period

Venkataramana Sridhar,[1,2] David B. Loope,[1]* James B. Swinehart,[1,2] Joseph A. Mason,[3] Robert J. Oglesby,[1,2] Clinton M. Rowe[1]

Spring-summer winds from the south move moist air from the Gulf of Mexico to the Great Plains. Rainfall in the growing season sustains prairie grasses that keep large dunes in the Nebraska Sand Hills immobile. Longitudinal dunes built during the Medieval Warm Period (800 to 1000 years before the present) record the last major period of sand mobility. These dunes are oriented NW-SE and are composed of cross-strata with bipolar dip directions. The trend and structure of the dunes record a drought that was initiated and sustained by a historically unprecedented shift of spring-summer atmospheric circulation over the Plains: Moist southerly flow was replaced by dry southwesterly flow.

Direct evidence of past changes in atmospheric circulation is largely absent from the geologic record. It is much easier to reconstruct indirect indicators of circulation such as vegetation, temperature, and precipitation. Episodically active dunes are an exception to this, however. Periods of dune activation and stabilization have frequently been used to infer alternating periods of drought and pluvial conditions, but few studies have fully exploited the orientation, morphology, and internal structures of dunes to reveal the wind regime under which they formed. We have used those features to explore paleowind regimes from the North American Great Plains.

In spring and early summer, strong southerly-to-southeasterly winds sweep over the Gulf of Mexico and transport moisture for growing-season rains to North America's core (*1*–*3*). Today, this moisture sustains the vegetation that stabilizes extensive dunefields on the Great Plains. A distinctive set of NW-SE–trending, grass-stabilized longitudinal dunes occupies 7500 km^2 of central Nebraska (Fig. 1); these dunes formed only 800 to 1000 years ago, near the end of the Medieval Warm Period (MWP) (*4*, *5*).

Annual precipitation ranges from 60 cm in the eastern Sand Hills to less than 43 cm in the west; ~50% comes in May, June, and July (*1*). During the 1930s and 1950s droughts, only isolated blowouts formed in the Sand Hills. Historical accounts indicate that some dune crests were grass-free at times during the 19th century (*6*). The large size of stabilized dunes and the dunefield's great extent indicate that the region is prone to droughts far more severe than those in the historical record (*7*). Optically stimulated luminescence (OSL) ages from deep within the largest dunes extend to 15,000 years before the present (yr B.P.), but shallow core and outcrop samples from dunes and adjacent wetlands indicate an episode of dune migration 800 to 1000 yr B.P., when aridity was widespread and persistent across western North America (*8*–*16*).

Many modern deserts contain morphologically distinct generations of dunes with different trends (*17*). If the internal structure and age of each generation are known, changes in regional winds can be reconstructed (*18*). The modern wind regime in the Sand Hills is dominated by northerly winter winds associated with midlatitude cyclones and by southerly flow in spring and summer associated with anticyclonic return flow of moist air from the Gulf of Mexico.

Dunes orient themselves to maximize sand transport normal to their crests (*19*, *20*). In bidirectional flows, transverse dunes form if the divergence angle between flows is less than 90° or close to 180°; oblique or longitudinal dunes (both with linear morphology) form if the angular difference is between 90° and 165° (*19*). Crests of longitudinal dunes lie within 15° of the resultant transport vector, crests of oblique dunes lie between 15° and 75°, and crests of transverse dunes lie between 75° and 90° (fig. S1) (*19*). Using wind data from six meteorological stations in and near the Nebraska Sand Hills (Fig. 1), we used the computer program Trend (*19*, *21*) to calculate the trend and resultant sand-drift vectors of dunes that would form (if sand were free to move) at each site. Trends range from S70°W to S55°W (fig. S2). Angles between calculated dune trends and modern resultants range from 44° to 90° and show that modern winds would generate oblique and transverse dunes, both of which would migrate southeastward; internally, these dunes contain only southward-dipping cross-strata (Fig. 2).

Crests of Medieval dunes in the southeastern Sand Hills are oriented N65°W. These dunes are 12 to 15 m high and several km long, with 0.2-km spacing (fig. S3). Cross-strata have bimodal dip directions (both NE and SW; Fig. 2 and fig. S4), which is the key characteristic of longitudinal dunes (*22*). These structures indicate that the wind regime that shaped the dunes was not only bidirectional, but also that the two wind vectors were of nearly equal magnitude (Fig. 2). Elongate dunes commonly join to form "y junctions" that are trustworthy indicators of resultant sand-drift direction (*23*). Because y junctions in the southeastern Sand Hills open toward the WNW (fig. S3), the resultant sand-drift direction for the Medieval dunes was ESE (Fig. 2).

[1]Department of Geosciences, University of Nebraska, Lincoln, NE 68588–0340, USA. [2]School of Natural Resources, University of Nebraska, Lincoln, NE 68583–0758, USA. [3]Department of Geography, University of Wisconsin, Madison, WI 53706, USA.

*To whom correspondence should be addressed. E-mail: dloope1@unl.edu

Downloaded from www.sciencemag.org on May 28, 2010